Geological Society of America Bulletin

Deformational features and impact-generated breccia from the Sierra Madera impact structure, west Texas

Sarah Huson, Michael Pope, A. John Watkinson and Franklin Foit

Geological Society of America Bulletin 2011;123, no. 1-2;371-383
doi: 10.1130/B30183.1

Notes

Deformational features and impact-generated breccia from the Sierra Madera impact structure, west Texas

Sarah Huson[1,†], Michael Pope[2], A. John Watkinson[1], and Franklin Foit[1]
[1]*School of Earth and Environmental Sciences, Washington State University, Pullman, Washington 99164, USA*
[2]*Department of Geology and Geophysics, Texas A&M University, College Station, Texas 77843, USA*

ABSTRACT

Deformational features from the Sierra Madera impact structure, west Texas, were studied to estimate shock temperature and shock pressure values involved during its formation. Sandstone, limestone, and polymict impact-generated breccia samples occur within the central uplift. The sandstones host several shock-related deformational features including toasted quartz grains and planar microstructures (planar fractures and planar deformation features) in quartz. Zircon mineral grains separated from the sandstone samples provide evidence of shock deformation in the form of planar fractures and granular surface textures. Both sandstone and carbonate within the central uplift contain shatter cones, whereas polymict impact-generated breccia samples contain shatter cone fragments and clasts of mixed lithology. Most high-temperature features (e.g., high-temperature mineral phases and a melt sheet) typically associated with less eroded structures of similar size are lacking; however, some small (millimeter-size) possible devitrified glass clasts within polymict breccias occur at several locations. Deformational features within zircon mineral grains, shatter cones, and quartz grains with multiple planar microstructures record pressure and temperature conditions during the impact of ~3–20 GPa and postshock temperatures between 350 and >1000 °C. Deformational conditions during the impact event were almost certainly higher, given that erosion has presumably removed most of the more severely shocked rocks.

INTRODUCTION

A significant amount of information regarding shock-metamorphism deformation in meteorite-impacted target rocks and impact-generated deposits has been collected over the last 40–50 yr. Impact structures can contain a variety of shocked and unshocked clasts derived from underlying basement rocks and surface cover (Metzler et al., 1988; Stöffler et al., 1988), and these clasts may be included in multiple, complex breccia units associated with impact events. For example, the Devonian Alamo breccia contains nine different types of breccias formed during, and immediately subsequent to, the impact event (Warme, 2004). Mechanisms forming these breccias include: the impact event itself, debris falling into the excavated crater, repeated tsunamis, and the failure of the preexisting carbonate platform margin due to the meteorite impact event (Warme and Kuehner, 1998; Warme, 2004).

Recent studies have identified planar deformation features (PDFs) in zircon grains (Bohor et al., 1993; Glass and Liu, 2001; Wittmann et al., 2006; Austrheim and Corfu, 2009). PDFs are closed, narrow, parallel features of highly amorphous material generally oriented parallel to crystallographic planes within the host mineral (Stöffler and Langenhorst, 1994; Grieve et al., 1996; French, 1998). They commonly occur in quartz grains (Stöffler and Langenhorst, 1994) but also can occur in other silicate minerals such as zircon. In zircon, PDFs form only when shock pressures reach 40–60 GPa and are visible using transmission electron microscopy (TEM) (Leroux et al., 1999). Below ~40 GPa, microcracks or planar fractures (PFs) form parallel to zircon cleavage planes (Leroux et al., 1999). Observations using scanning electron microscopy (SEM) document increasing fracturing along cleavage planes and irregular fracturing on the micrometer scale with an increase in shock pressure (Leroux et al., 1999). In addition to PDFs and PFs, granular textures in zircon grains have been identified from mid-sized (~20 km diameter) to larger (>~90 km diameter) impact structures (i.e., Ries, Popigai, Sudbury, Chicxulub, Manicouagan, Chesapeake Bay; Bohor et al., 1993; Glass and Liu, 2001; Wittmann et al., 2006). Impact-deformed zircon grains are documented in the Ries (23 km in diameter; Wittmann et al., 2006), Gardnos (6 km in diameter; Kalleson et al., 2009), and Lappajärvi (17 km in diameter; Mänttäri and Koivisto, 2001) impact craters.

Shatter cones are another unique impact-produced feature. Shatter cones consist of a fracture surface characterized by striations diverging from cone apex to base formed by the passage of a shock wave through rock. Originally, the cone was thought (Dietz, 1968; Wilshire et al., 1972) to point in the direction from which the shock wave was generated, i.e., the point of contact between the impactor and target rock. However, a study of shatter cone fracturing and orientations within impact craters (Wieland et al., 2006) suggests the formation of these features is more complicated and is still not completely resolved.

Many impact cratering studies have concentrated on understanding deformation in siliciclastic minerals because of the relative abundance and robust nature of quartz at Earth's surface (French, 1998). Yet, not all impact structures contain quartz-bearing rocks. Therefore, pressure and temperature deformation results based on quartz are not applicable to all impact structures, since ~30% of all terrestrial impact structures formed primarily in carbonate rocks (Grieve and Robertson, 1979; Grieve and Pesonen, 1996). Consequently, in structures containing little siliciclastic material, it is somewhat more difficult to determine pressure and temperature conditions of an impact. However, impact structures containing both siliciclastic and carbonate rocks can provide a bridge to understand shock-induced deformations in both rock types. Well-studied carbonate and mixed siliciclastic and carbonate structures include Meteor crater (diameter 1.2 km) in Arizona (Kieffer et al., 1976; Burt et al., 2005), the Steinheim and Ries

[†]E-mail: sahuson@hotmail.com

GSA Bulletin; January/February 2011; v. 123; no. 1/2; p. 371–383; doi: 10.1130/B30183.1; 9 figures; 2 tables.

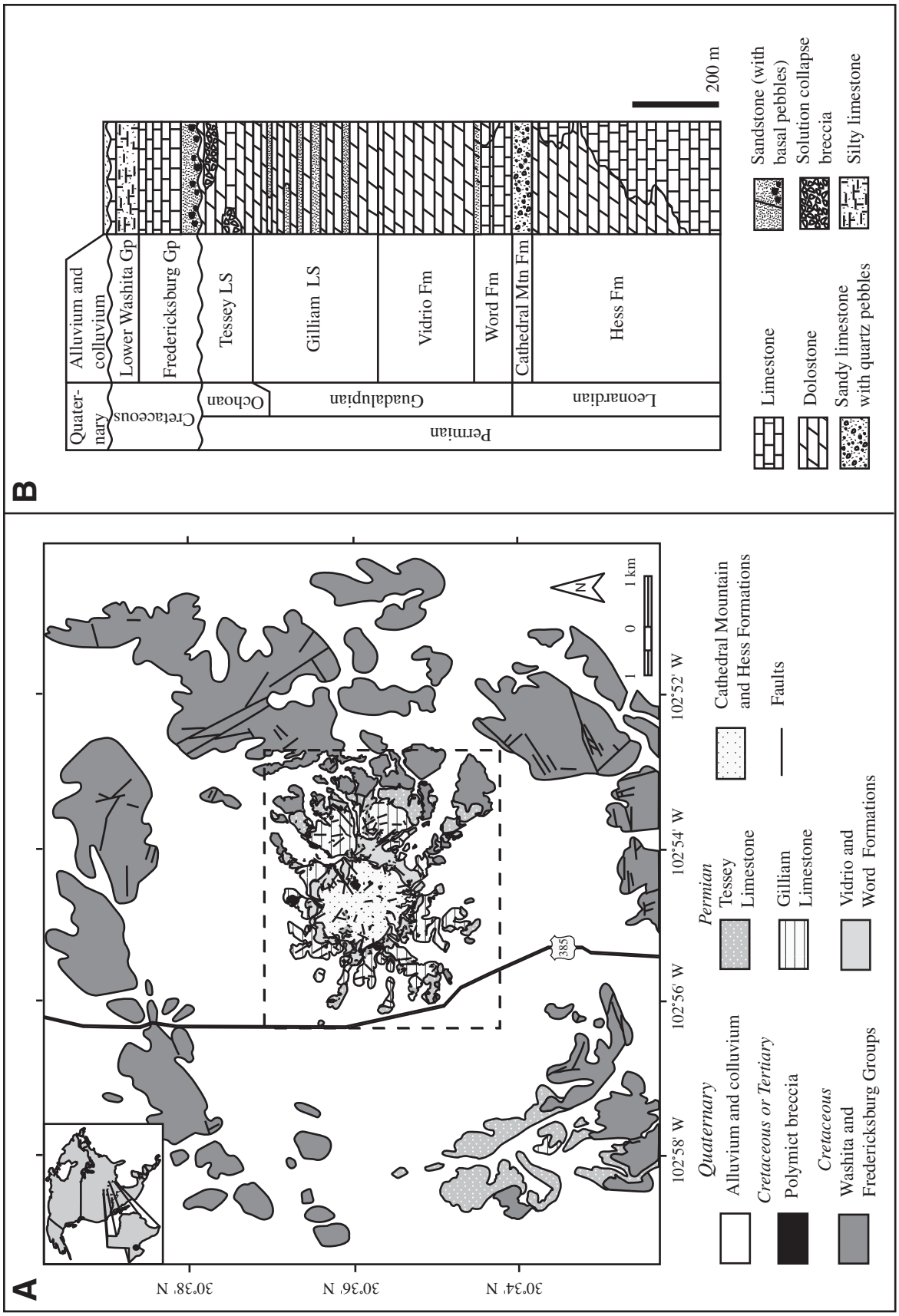

Figure 1. (A) Geologic map of Sierra Madera impact crater (modified from Wilshire et al., 1972). Dashed box in center indicates region shown in Figures 5 and 6. (B) Stratigraphic column for rocks exposed at Sierra Madera.

structures in Germany (diameters of 3.8 km and 24 km, respectively; Graup, 1999; Skála and Jakeš, 1999), and the Haughton structure in Canada (diameter of 24 km; Osinski and Spray, 2001; Osinski, 2007).

Studies of impact structures formed in carbonate-rich rocks have also focused on cratering products. For example, carbonate rocks in impact structures can contain high-temperature melts and carbonate-silicate immiscibility features (i.e., Ries and Haughton structures; Graup, 1999; Osinski and Spray, 2001; Tuchscherer et al., 2004).

The Sierra Madera impact structure is a well-exposed complex impact structure with a diameter of 12.9 km, last studied in the late 1960s (Wilshire et al., 1972). Target rocks at Sierra Madera are predominantly late Paleozoic and Mesozoic carbonate rocks with a few interbedded siliciclastic units. We reexamined the impact-deformed rocks from Sierra Madera to better understand deformational products associated with a medium-sized carbonate structure and to provide data in a critical intermediate size and energy range for which information currently is lacking. We present here new descriptions of impact-generated breccia, the possible identification of shock-related deformations in zircon, and descriptions of shatter cones. Using these features, we estimate the temperature and pressure conditions during the impact event and relate the occurrence and distribution of these features to the current crater erosional level for this impact structure.

GEOLOGIC SETTING

The Sierra Madera impact structure near Fort Stockton, Texas (Fig. 1), is a well-exposed, eroded remnant of a complex impact crater (Eggleton and Shoemaker, 1961; Wilshire and Howard, 1968; Howard et al., 1972; Wilshire et al., 1972). The central uplift at Sierra Madera is composed of steeply dipping, folded, and faulted Upper Paleozoic to Cretaceous carbonate and siliciclastic rocks. Upper Permian carbonate and siliciclastic strata include the Hess, Cathedral Mountain, Word, and Vidrio Formations, and the Gilliam and Tessey Limestones (Table 1). Lower Cretaceous rocks of the Fredericksburg and Lower Washita Groups, composed of mixed carbonate and siliciclastic rocks, are exposed along the eastern margin of the central uplift. The carbonate Permian Hess Formation, the oldest stratigraphic unit exposed in the central uplift, was displaced vertically at least 790 m during the excavation and modification stage of crater development (Wilshire et al., 1972). Impact-generated polymict and monomict breccias occur within and crosscut target rocks of the central uplift of the structure. The crater rim at Sierra Madera is composed of Lower Cretaceous carbonate and siliciclastic rocks of the Fredericksburg and Lower Washita Groups. On the southwest side of the rim, rocks from the Upper Permian Gilliam and Tessey Limestones are exposed. Cretaceous strata occur ~30–60 m above the alluvium-filled ring depression. Strata on the rim generally dip 0°–5° radially, though at some locations, dip can be as great as 30°. Postimpact erosion has removed an estimated ~600 m of material on the crater rim (Wilshire et al., 1972).

METHODS

We mapped, sampled, and carefully described impact-generated breccias from Sierra

TABLE 1. STRATIGRAPHIC UNITS EXPOSED WITHIN AND SURROUNDING SIERRA MADERA IMPACT STRUCTURE

Stratigraphic unit	Description
Alluvium Quaternary	0–15 m of unconsolidated boulder- to silt-size, angular to rounded clasts of dolomite, limestone, chert, and sandstone, locally well-cemented as caliche (Wilshire et al., 1972).
Fredericksburg and Lower Washita Groups Lower Cretaceous	The lower part of the Fredericksburg consists of the Maxon Sandstone, a 15–30-m-thick red-brown, fine- to coarse-grained silica-cemented sandstone. The Edwards Limestone (40–60 m thick) is a platy, light gray and brown limestone. The Kiamichi Formation (~15 m thick) is a thin-bedded, light-gray limestone. The lower Washita Group consists of platy to massive, medium-grained, shaly limestone. The Fredericksburg and Washita Groups represent deposition in a fluvial/deltaic to shallow-marine setting (Hill, 1996) and are not differentiated at Sierra Madera due to poor exposures and lack of stratigraphic control.
Tessey Limestone Upper Permian	0–120-m-thick, gray brown dolomite with sparse fossils. In some locations, this unit contains areas of solution-collapse breccia composed of laminated small (centimeter-size) to large (several-meter-size) fragments of limestone-cemented mosaic-like with calcite and/or dolomite cement. This unit is unconformable with the underlying Gilliam Limestone. Deposition occurred in a hypersaline basin that underwent periods of subtidal to supratidal deposition and subaerial exposure (Haneef and Wardlaw, 2000). Meteoric dissolution created karst features and collapse breccias (Hill, 1996). These breccias occur on the east side of the central uplift (Wilshire et al., 1972).
Gilliam Limestone Upper Permian	213–290-m-thick, light-colored dolomite interbedded with calcite-cemented fine-grained sandstone; sandstone layers pinch out laterally and are discontinuous. This unit is conformable with the Vidrio Formation. The Gilliam Limestone was deposited in a lagoonal and back-reef setting (Hill, 1996).
Vidrio Formation Lower Permian	60–230-m-thick massive to thick-bedded dark dolomite with sparse fossils. Rounded chert nodules are common often and gray-colored with an orange weathering rind. The original rock fabric and fossils of this unit are difficult to characterize and interpret; thus the depositional environment at Sierra Madera is unknown. However, in other parts of the Delaware Basin, the Vidrio Formation records initial reef development, though the reef facies is not seen at Sierra Madera (Hill, 1996).
Word Formation Lower Permian	0–86-m-thick dolomitized limestone divided into two members. The lowermost member is an unnamed limestone unit, 0–76 m thick (Wilshire et al., 1972). It contains thin- to thick-bedded limestone, with crinoid and fusulinid fossils, and some interbedded finely crystalline dolomite. The upper sandstone member (0–10 m thick) consists of interbedded coarse-grained sandstone with silicified crinoid stems and silty to fine-grained sandstone with calcite cement. Locally, this unit grades laterally to a sandy dolomite. The depositional setting for the Word Formation is controversial, being either basinal with turbidity currents moving clastics off the shelf (Ross, 1986) or a shallow-water lagoon (Rohr et al., 1982; Wardlaw et al., 1990).
Cathedral Mountain Formation Lower Permian	0–24-m-thick conglomerate containing chert and quartz pebbles in a dolomite matrix (Wilshire et al., 1972). Beds of cross-bedded coarse, quartz sandstone occur locally as lenses. This unit grades conformably upward into the lower part of the Word Formation. The depositional environment was a shallow-water deltaic complex (Wardlaw et al., 1990) or basinal where clastics are derived from debris flows or turbidity currents (Ross, 1986).
Hess Formation Lower Permian	730–850-m-thick, fine-grained, medium- to thick-bedded limestone and dolostone interbedded with sandstone, siltstone, and shale. Sediments were deposited in a shallow-water lagoon. Common fossils include fusulinids, brachiopods, and bryozoa. There is a gradual up-section decrease in clastic material and increase in dolomite in this unit. At Sierra Madera, 365–430 m occur at the surface, and the unit gradually increases in thickness to the north (Wilshire et al., 1972).

Madera to determine their distribution and formation processes. Characteristics such as texture, clast composition, possible melt products or glasses, deformational features in minerals, and flow features within breccias are described. Studies of the target rocks include shatter cone outcrop, characteristics and fracture patterns, carbonate response to shock conditions, and deformation in quartz and other minerals. We examined 122 thin sections of target rocks, with and without shatter cones, and impact-generated breccias from the central uplift of Sierra Madera using a petrographic microscope. Sixty-three selected thin sections were analyzed for evidence of melt features using plane light microscopy and scanning electron microscopy (SEM). Carbon-coated, polished thin section slides were analyzed using SEM with backscatter electron (BSE) imagery and energy dispersive spectrometry (EDS) to distinguish silica-rich phases from carbonate material. Samples were analyzed using a Zeiss LEO982 FE-SEM. Beam operating conditions were 20 kV and ~1 nA, with an operating distance of 10 mm. The Oxford INCA EDS system was used for chemical information. A copper standard was used to collect a peak to make sure the spectrometer was working properly and was identifying the correct peaks. The SEM used in this study is housed at the Pacific Northwest National Laboratory in Richland, Washington.

We also document possible shock-induced surface textures on zircon grains from Permian sandstones within the central uplift. Zircon grains separated from sandstone in the central uplift were examined for shock deformation features and were used in the determination of the age of the impact event using fission-track analysis. Sandstone samples were collected from the Maxon Sandstone, sandstone beds of the Permian Gilliam Limestone, and the sandstone member of the Permian Word Formation. Sandstone samples were crushed, and zircon grains (<100 μm) were separated using a Gemini table, magnetic separator, and heavy liquid separation (methylene iodide) after the mineral separation techniques of Donelick et al. (2005). Fractions for petrographic microscopy investigations were mounted in epoxy, polished to half-grain, and studied under the microscope under high magnification using both transmitted and reflected light. Zircon fractions for SEM analysis were etched with a saturated solution of NaOH at 70 °C for 1.5 h to reveal shock features after Bohor et al. (1993). These grains were mounted on SEM stubs and carbon coated prior to SEM analysis. Beam operating conditions were 2 kV and ~100 pA, with an operating distance of 4 mm.

DEFORMATIONAL FEATURES

Target Rocks

Deformations in Quartz Grains from Carbonate-Cemented Sandstones

There are four different sandstone units exposed at the Sierra Madera impact structure; from oldest to youngest they are the Permian Cathedral Mountain Formation, a sandstone member of the Permian Word Formation, sandstone within the Permian Gilliam Limestone, and the Cretaceous Maxon Sandstone. Thin sections used for sandstone analysis include two for the Cathedral Mountain Formation, four for the Word sandstone, five for the Gilliam sandstone, and two for the Maxon Sandstone. All units contain shock-induced planar microstructures within quartz grains (Fig. 2).

The Cathedral Mountain Formation is characterized by 0.1–0.2 mm quartz grains within a carbonate matrix. Typically, quartz grains are not in contact with one another. Deformation in these quartz grains includes grain fracturing, grain partitioning, and quartz grains with undulose extinction. Planar microstructures occur in 5%–10% of all the quartz grains. Less than 5% of all quartz grains with planar microstructures are "toasted," where the quartz has a grainy brown appearance due to an increase in vesicles or fluid inclusions in some shock metamorphosed quartz grains, which cause the scattering of transmitted light (e.g., Short and Gold, 1996; Whitehead et al., 2002; Ferrière et al., 2009).

Similar to the Cathedral Mountain Formation, the sandstone member of the Word Formation is a carbonate cemented rock with 0.1–1.6 mm quartz grains dispersed in a carbonate matrix. Grain fracturing and suturing along long contacts are very common, as is undulose extinction and grain partitioning. Planar microstructures occur in less than 10% of all quartz grains. Between 5% and 10% of those grains containing planar microstructures also have a toasted appearance (Fig. 2A).

The sandstone of the Gilliam Limestone contains the most shock features at Sierra Madera. Silty sand units within Gilliam are characterized by 0.04–0.1-mm-size quartz grains that

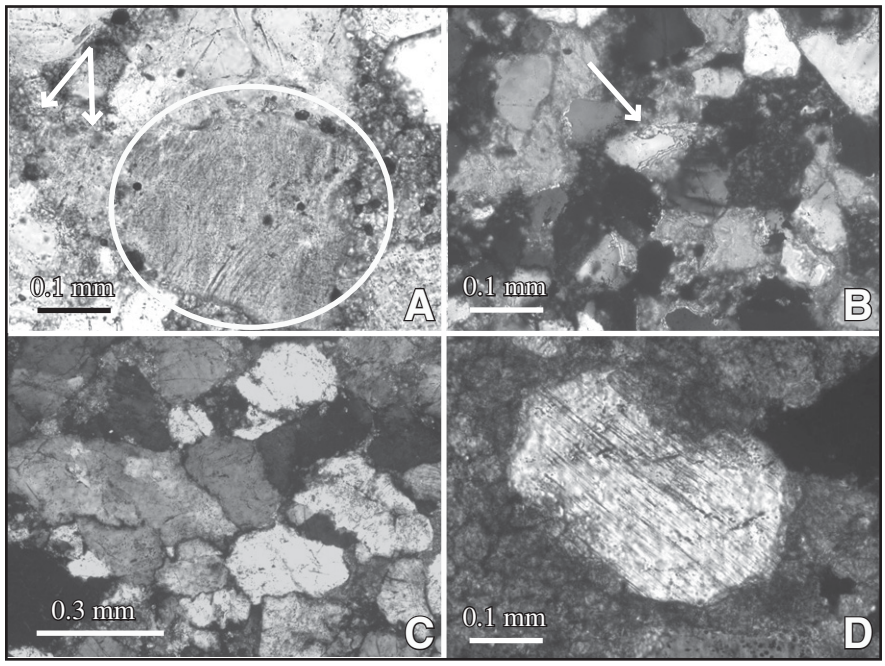

Figure 2. Photomicrographs of sandstone deformation in the Sierra Madera impact structure. (A) Toasted quartz from the Gilliam Limestone (see circle). Arrows indicate planar microstructure directions. Note darkening, blotchy appearance. Plane-polarized light. (B) Symplectic texture between quartz grains from the sand-rich unit of the Gilliam Limestone. Note areas of high birefringence around the rims of quartz grains (see arrow). Cross-polarized light. (C) Jigsaw texture between quartz grains from the Maxon Sandstone. Cross-polarized light. (D) Planar microstructures in quartz from the Word Sandstone. Cross-polarized light. Sample locations for these images are noted by square symbols on Figure 6: 1—Fig. 2A; 2—Fig. 2B; 3—Fig. 2C; 4—Fig. 2D.

are grain supported. The grains are closely packed, and carbonate material is reduced to a microbreccia. This interlocking grain texture was termed "jigsaw" by Kieffer (1971). Quartz grains are highly fractured (both irregular and planar), commonly have undulose extinction, and contain grain partitioning. Symplectic regions between quartz grains were identified by their high birefringence and opaque regions in plane light (Fig. 2B). Planar microstructures occur in 15% of quartz grains; 5% of all quartz grains with planar microstructures are toasted.

The Cretaceous Maxon Sandstone of the Lower Fredericksburg Group is characterized by 0.04–1.2 mm fluid inclusion–rich quartz grains with carbonate cement. The sand grains in this unit have a jigsaw texture of interlocking quartz grains similar to those in the Gilliam Limestone sandstone bed (Fig. 2C). Quartz grains typically also display undulose extinction, fractures, and grain partitioning. Approximately 5% of all quartz grains have decorated planar microstructures (Fig. 2D), with >5% of these being toasted.

Deformation in Carbonate Rocks

Shock-induced deformation is not apparent in all carbonate-rich rocks within the central uplift. In thin section, most carbonate rocks are fine-grained and contain fractured fossil and microfossil fragments. Stylolites are common in the Word Formation. All carbonate formations display shatter cones. Shock deformation in carbonate rocks was studied using X-ray diffraction (Huson et al., 2009). Shocked carbonate-rich rocks from the central uplift were compared with unshocked rocks from outside the crater using XRD peak patterns and Rietveld refinement of full-width at half-maximum (FWHM) peak values. It was possible to distinguish impact shocked rocks from comparable unshocked rocks since shocked samples have broader peak patterns and greater Rietveld FWHM values for higher 2θ values (Huson et al., 2009).

Deformations in Zircon Grains

Zircon mineral grains separated from the sandstone members of the Word Formation and the Gilliam Limestone within the central uplift of Sierra Madera also display evidence of shock damage (Fig. 3). Parallel features on polished mounts of zircon grains were documented in Permian sandstones using transmitted light microscopy (Fig. 3A; Huson et al., 2005). The lineations occur in the interior of the zircon grains and are tentatively called planar fractures, since they have not been properly characterized using, e.g., transmitted electron microscope or U-stage. These features are not abundant and occur in less than 5% of the samples studied.

Zircon grain surfaces also were studied using SEM to document shock-induced deformation. Three types of textures were documented on rounded and euhedral zircon grains: (1) smooth and seemingly unshocked, (2) planar features, and (3) a granular texture. Most smooth zircon grain surfaces showed no signs of shock deformation. Of the ~400 zircon grains studied, fewer than 5% of the zircon surfaces showed either planar features (7 grains) or a granular texture (12 grains; Figs. 3B and 3C). These features are texturally similar to those reported for zircon from the Cretaceous-Tertiary (K-T) boundary ejecta layer, as well as the Chesapeake Bay, Ries, Chicxulub, and Popigai structures (Bohor et al., 1993; Glass and Liu, 2001; Wittmann et al., 2006).

Shatter Cones

Shatter cones are unique impact-produced fracture surfaces characterized by diverging striations from cone apex to base (Dietz, 1968). They have two basic morphologies, a flat striated surface of cones that overlap like shingles and complete to partial three-dimensional cones (Dietz, 1968; French, 1998; Wieland et al., 2006).

Shatter cones were discovered at Sierra Madera in 1959 (Dietz, 1960; Kelly, 1966) and are abundant within a 2 km radius from

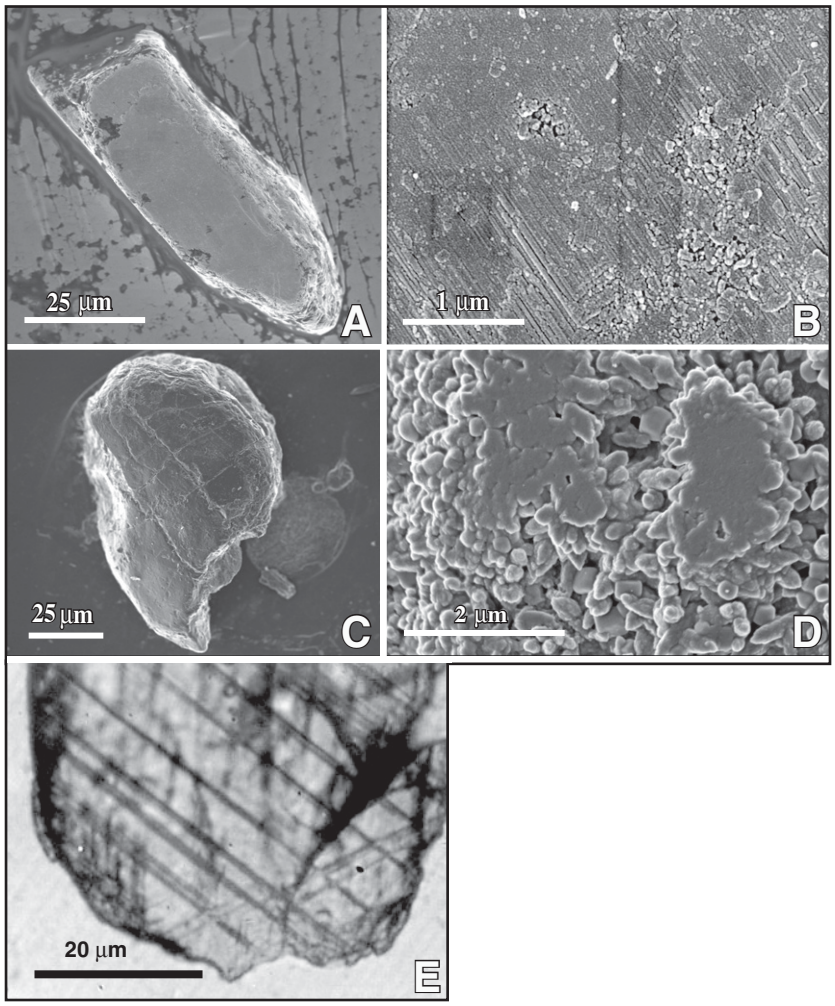

Figure 3. Possible deformation in zircon. (A–B) Scanning electron microscope (SEM) images of possible surface expression of planar features in zircon from the Word Sandstone. (C–D) SEM images of granular texture in zircon with remnant patches of the original smooth surface from the Word Sandstone. (E) Light microscopic image of planar features from a polished zircon embedded in epoxy. Zircon sample is from the Gilliam sandstone. Sample locations for these images are noted by squares on Figure 6: 5—Fig. 3A–D; 6—Fig. 3E.

the center of the central uplift (Howard and Offield, 1968; Wilshire et al., 1972). Shatter cones occur in all Permian carbonates but are most common in the Gilliam Limestone, Vidrio, Word, and Hess Formations (Fig. 4). They also occur within the sandstone member of the Word Formation, sand units within the Gilliam Limestone, and are weakly developed in the Cathedral Mountain Formation (Fig. 4A). Cone fragments are also reported in well cuttings at a depth of 1600 m (suspected cone fragments to a depth of ~3657 m) beneath the central uplift (Howard and Offield, 1968; Wilshire et al., 1972). Cone sizes range from 1 cm to ~45 cm in height and 0.5 cm to ~20 cm in diameter (Wilshire et al., 1972). Both cone morphologies, flat surfaces and three-dimensional cones, occur at Sierra Madera (Wilshire et al., 1972), and while linear striations and typical shatter cone morphologies are most common, curved striations and irregular cones are also present (Fig. 4B). Shatter cones are not uniformly developed in all units of the central uplift and may occur at one location but not occur in the same formation at a different location.

Small, centimeter-sized shatter cones within the Gilliam Limestone have a distinct weathering fracture pattern (Fig. 4C). When broken, blocks of this unit contain many small complete shatter cones. This appearance results from weathering along shatter cone fractures, although the exact relationship is not well understood.

After reorientation of beds containing shatter cones to their original position at Sierra Madera, the shatter cones generally point toward the center of the impact structure. However, it is not uncommon for cones to be oriented in directions other than toward the crater center (Fig. 5). Additionally, some shatter cones are oriented in different, sometimes opposite directions within the same sample (Fig. 4D). Similar shatter cone

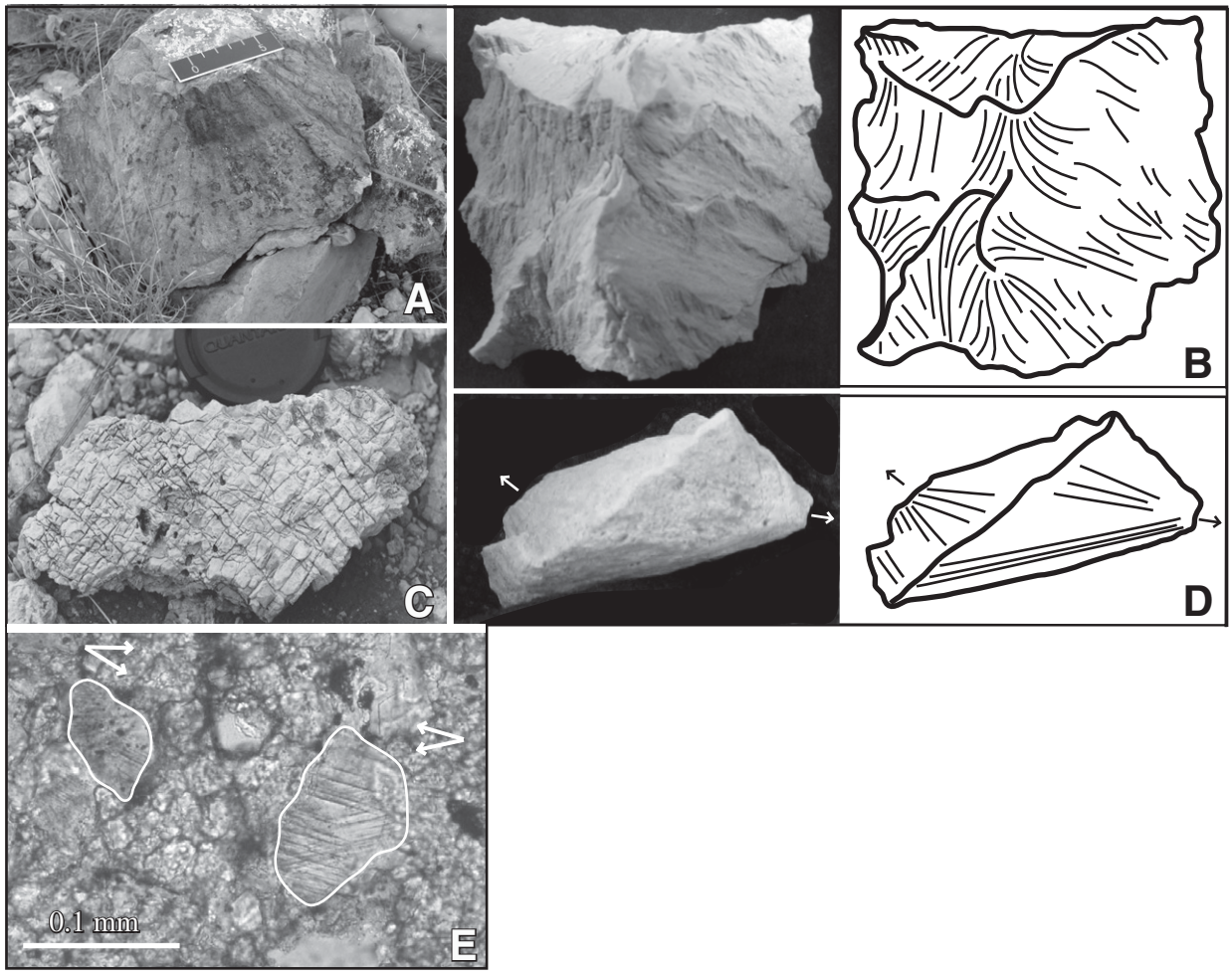

Figure 4. Shatter cone deformation. (A) Shatter cone in sandstone from the Gilliam Limestone. Scale bar is in cm. (B) Photograph and line-drawing of curved, irregular shatter cone from the Gilliam Limestone. Sample is 8.5 cm in width. (C) Distinct weathering fracture pattern of Gilliam Limestone sample containing centimeter-scale shatter cones. Lens caps is 5 cm in width. (D) Photograph and line-drawing of shatter cones oriented in opposite directions within the Hess Formation. Arrows point in direction of cone apex. Sample is 4 cm in length. (E) Photomicrograph showing toasted (left grain) and untoasted (right grain) quartz grains (outlined) from a shatter cone in the Gilliam Limestone. Note two directions of planar microstructures within both grains (arrows) and overall darkening of the toasted grain. Plane-polarized light. Sample locations for these images are noted by the square symbols on Figure 6: 7—Fig. 4A; 8—Fig. 4B; 9—Fig. 4C; 10—Fig. 4D; 11—Fig. 4E.

observations are reported from the Haughton structure (Osinski and Spray, 2006).

Thin sections of shatter cones reveal that they are composed of fine-grained carbonate and silt- to sand-sized quartz grains. Quartz deformation features in shatter cones include planar microstructures, grain fracturing, and toasting (Fig. 4E). Deformational features such as twinning or brecciation are not obvious within the carbonate material of the shatter cones.

Breccias

Four breccia units occur within the Sierra Madera impact structure: impact-generated monomict and polymict breccias, an evaporite collapse breccia within the Tessey Limestone, and modern day caliche (Table 2). Impact-generated breccias were first identified at the Sierra Madera impact structure (Fig. 6) by Wilshire et al. (1972). The first, called a "monolithic breccias," is characterized by an in situ shattering of rock of a single lithology. The second breccia, termed "mixed breccias," contains clasts of two or more lithologies in a fine-grained carbonate matrix. We use the terms "monomict impact breccia" and "polymict impact breccia" to refer to Wilshire et al.'s (1972) breccia types after the terminology of Stöffler and Grieve (2007). Evaporite collapse breccia in the Tessey Limestone is characterized by mosaic-like cementing of

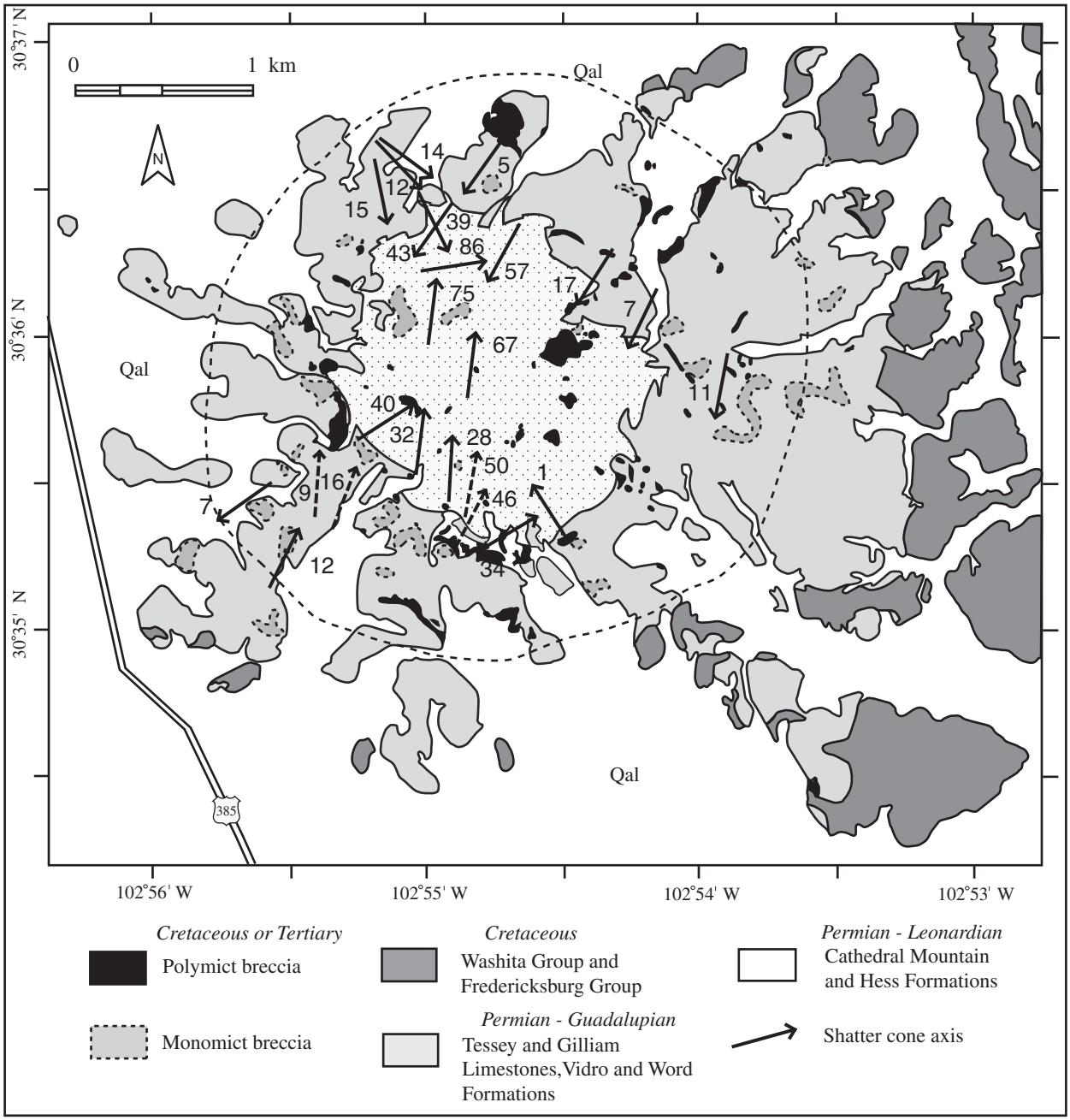

Figure 5. Geology map of the central uplift of the Sierra Madera impact crater. Numbers next to arrows indicate the orientation of shatter cones in beds restored to horizontal position. Dashed circle indicates extent of abundant shatter cones. Figure includes data from Wilshire et al. (1972; solid arrows) and this study (dashed arrows).

TABLE 2. COMPARISON OF BRECCIA TYPES AT SIERRA MADERA

Breccia type	Description	Matrix/cement	Size range of clasts	Clast types	Clast shape	Outcrop shape	Distribution of outcrops	Shock indicators	Interpretation
Monomict	Intensely shattered clasts of a single lithology	Fine-grained matrix material same as clasts	Millimeter to centimeter	Very localized	Rounded and angular, in central uplift	Irregular	Random	None	Shock wave–induced in situ fracturing with little or no rotation of clasts. Local to Sierra Madera.
Polymict	Clasts of two or more lithologies	Fine-grained carbonate matrix	Millimeter to meter	Very localized	Rounded and angular, in central uplift	Irregular, tabular and crosscutting (dikes)	Random	Shatter cones, possible melt material	Shock wave–induced breccia composed of all rock types from Sierra Madera. Local to Sierra Madera.
Collapse	Mosaic-like cementing of angular, laminated dolomite clasts	Dolomite matrix and regions with drusy calcite cement	Millimeter to meter	Tessey Limestone	Angular	Irregular	Mostly east side	None	Cementing of clasts within solution-collapse cavities. Occurs regionally outside of the crater (Hill, 1999).
Caliche	Rounded clasts of differing compositions cemented together	$CaCO_3$ layered cement	Millimeter to centimeter	Every rock type exposed at the surface	Rounded–angular	In situ and irregular	Slope wash, ephemeral streams	None	$CaCO_3$ crust cementing material in slope wash. Occurs in desert and arid regions.

angular, laminated dolomite clasts. Deposition occurred in a hypersaline basin that underwent periods of subtidal to supratidal deposition and subaerial exposure (Haneef and Wardlaw, 2000). Meteoric dissolution created karst features and collapse breccias (Hill, 1996). The evaporite collapse breccia in the Tessey Limestone is distinguishable from monomict impact breccia by the presence of detrital quartz within the matrix and its widespread occurrence outside of the crater (Wilshire et al., 1972; Hill, 1996).

Caliche, common in arid regions of the southwest United States, is a carbonate crust that cements material in slope wash and ephemeral stream channels. At Sierra Madera, it can be easily confused with polymict impact breccia because both breccia types contain clasts of several compositions. However, in thin section, the cement in caliche is layered, reflecting numerous, slow cementation events within the matrix and surrounding clasts over time, whereas the cement-matrix in polymict impact breccia is massive.

Monomict Impact Breccia

Monomict impact breccias occur as pod-like lenses in all Permian carbonate formations and the Lower Cretaceous Maxon Sandstone within the central uplift of Sierra Madera. Irregular zones of brecciation are randomly distributed throughout the central uplift (Fig. 6). At some locations, breccias show little clast rotation and appear as fractured bedrock (Fig.7A). In other locations, the breccia contains a large amount of matrix material producing rough and irregular outcrops (Figs. 7B and 7C). Monomict impact breccia in thin section is characterized by intensely shattered clasts within a dark fine-grained matrix. Shattered clasts are either broken in place with matrix-filled cracks between well-defined fragments, or clasts show some movement with less distinct edges and the surrounding matrix contains internal flow foliation. The dark fine-grained matrix within monomict impact breccia was previously identified as mylonite (Wilshire et al., 1972).

Polymict Impact Breccia

Impact-generated polymict breccias crosscut in all formations in the central uplift of Sierra Madera (Fig. 8A). Outcrops occur parallel or perpendicular to bedding as dikes, pod-like lenses, or tabular sheets and may or may not be associated with faults (Wilshire et al., 1972). The three-dimensional configuration of breccia in the subsurface is not well understood. For example, it is not clear if the outcrops are connected by a network of pipes or if each outcrop is a single occurrence of breccia. Polymict breccia is found only within the central uplift and is not found on the crater rim. The largest outcrop

by area (~200 m by ~250 m) occurs on the western flank of one of the northern ridges of the central uplift (Fig. 6).

Polymict breccia clasts are derived from all rocks exposed at the surface of the structure in a tan to reddish fine-grained carbonate matrix. Clast size ranges from millimeter to meter sized. Depending on the location of the breccia, one outcrop may be enriched with clasts from a particular formation when compared to other breccia outcrops. Carbonate clasts within the polymict breccia contain small fractures filled with a fine-grained dark carbonate material. Sandstone clasts within the polymict breccia contain toasted quartz, and quartz grains have multiple planar microstructures, up to two sets under the petrographic microscope. Shatter cones occur in some limestone and chert clasts within polymict breccia (Fig. 8D). Quartz grains within shatter cone clasts contain multiple planar microstructures and are highly toasted. Polymict breccias also contain sandstone clasts that are melted and display flow textures (Figs. 8E and 8F). Possible devitrified silica glass within polymict breccia occurs as clear or light brown to partially opaque irregular blebs (Fig. 8G). These clasts do not occur in all polymict breccia

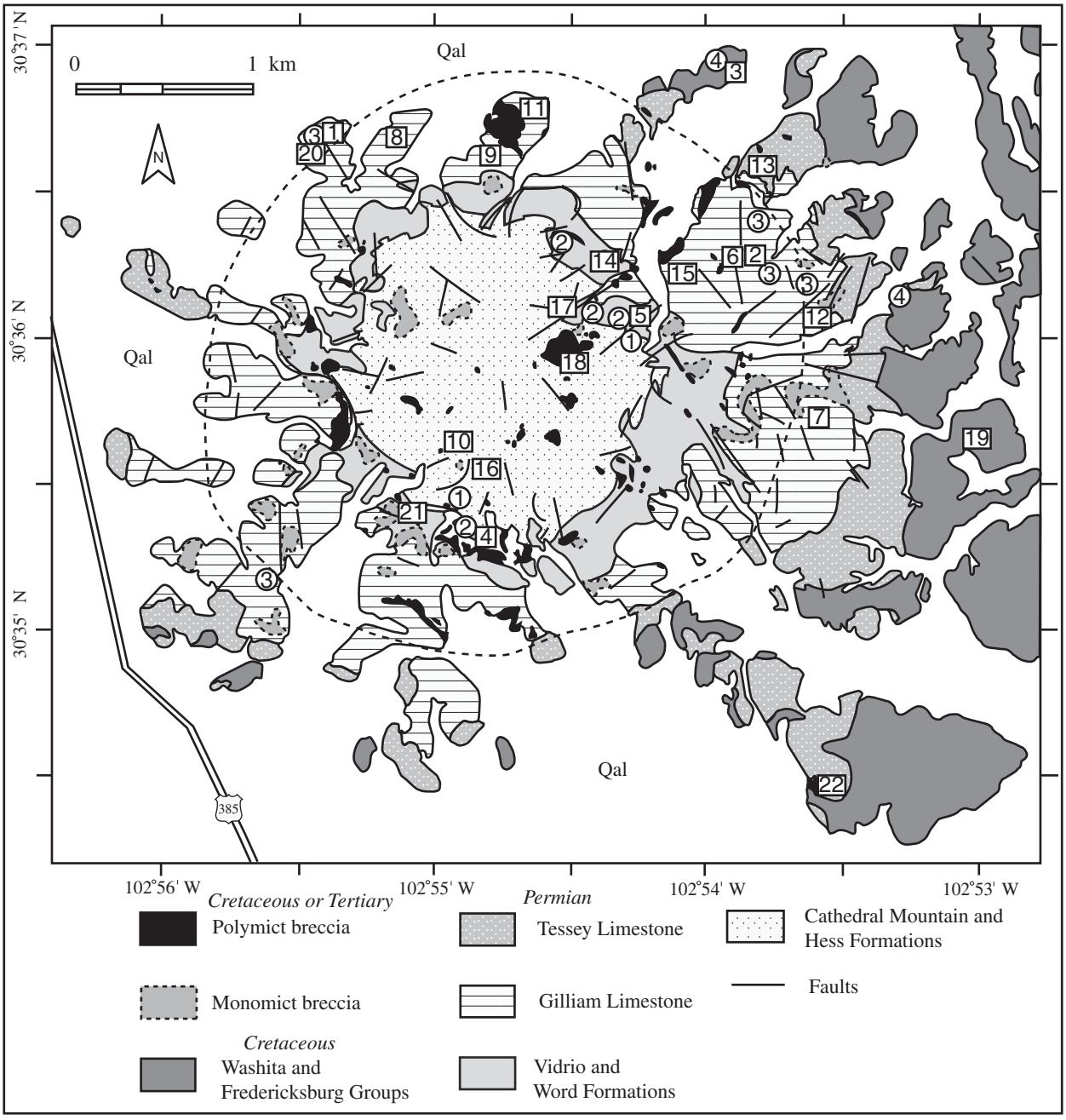

Figure 6. Geologic map of the central uplift of Sierra Madera showing location of breccia types (modified from Wilshire et al., 1972). Dashed circle indicates extent of abundant shatter cones. Circles with numbers indicate sandstone sample locations: 1—Cathedral Mountain Formation, 2—Word sandstone, 3—Gilliam sandstone, 4—Maxon Sandstone. Squares with numbers indicate sample locations for Figures 2–8.

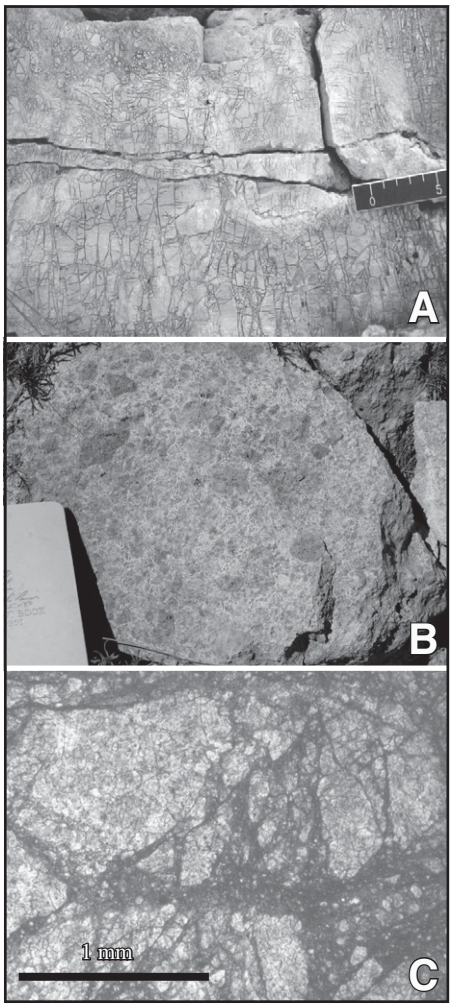

Figure 7. Monomict impact breccia from Sierra Madera. Monomict impact breccia is characterized by fracturing and internal chattering of clasts with fine-grained material between larger coherent clasts. (A) Monomict breccia within the Gilliam Limestone with little clast rotation and small amounts of matrix between clasts. Scale bar is in cm. (B) Monomict impact breccia within the Tessey Limestone with a large amount of matrix between clasts. Note irregular rough appearance of outcrop. Field book is 15 cm in length. (C) Photomicrograph of monomict impact breccia within the Word Formation. Plane-polarized light. Sample locations for these images are noted by square symbols on Figure 6: 12—Fig. 7A; 13—Fig. 7B; 14—Fig. 7C.

samples or locations. Devitrified silica glass is present as fragments within polymict breccias, and it occurs as less than 5% of the clasts. Carbonate melt or "quenched" material was possibly identified at one location within the central uplift (Fig. 8H). This material is a fine-grained dark orange carbonate. In thin section, the material contains small clasts that are unmelted and partially melted. Partially melted clasts are identified by having a coarse crystalline texture that gradually becomes more aggregate-like. Using SEM, possible carbonate-silicate immiscibility features were identified (Fig. 8I). When rapidly quenched, carbonate material forms either a holocrystalline material or an aggregate of fine-grained carbonate (Graup, 1999).

Small (5–15 cm in diameter) injection dikes of polymict breccia intrude the host limestone (Fig. 8B). Clasts within the dikes are rounded to subangular and smaller in size (millimeters) than clasts within pod-like or tabular breccia outcrops. Dike material contains little clastic material, and the carbonate matrix has a finer texture than the host rock (Fig. 8C).

DISCUSSION

Zircon Data

SEM work on zircon mineral grains from the Sierra Madera impact structure led to the possible identification of two different impact-related textures. Less than 5% of the zircon grains studied showed either planar fracturing or a granular texture. Zircons exposed to shock pressures below 20 GPa do not develop shock deformational features (Wittmann et al., 2006). On the TEM scale, planar microstructures begin to form at 20 GPa with well-developed planar microstructures forming between 40 and 60 GPa (Leroux et al., 1999; Wittmann et al., 2006). Granular textures form at ~50 to ~70 GPa (Wittmann et al., 2006). Zircon observations for this study were on the SEM scale and not TEM scale, and therefore the deformational features within zircon were recorded as enhanced fracturing along cleavage planes. Therefore, zircon textures from Sierra Madera indicate that shock pressures during the impact event were at least ~20 GPa if the cleavage fracturing was enhanced by shock wave propagation from the impact event.

Shatter Cone Data

Multiple directions of shatter cones and irregular cone shapes indicate that the method of formation for these features was complex. Both full and partial three-dimensional (3-D) cones as well as the overlapping, shingle morphologies are present within the central uplift as cones within target rocks and clasts within polymict breccia. The distinct weathering pattern of shatter cones within the Gilliam Limestone may correspond to a centimeter-sized joint or fracture pattern within the rock where erosion is occurring along weakened fracture planes. The fracture pattern within the Gilliam Limestone may be similar to the multiply striated joint surfaces at the Vredefort structure, where the authors associated striated surfaces and jointing to the occurrence of shatter cone formation (Nicolaysen and Reimold, 1999; Wieland et al., 2006). Detailed mapping of the multiply striated joint surfaces and shingle morphology shatter cones will lead to a better understanding of impact-induced fracturing in the target rocks.

Previous researchers have favored a relatively late formation of shatter cones with regard to multiply striated joint surfaces (Nicolaysen and Reimold, 1999). At Sierra Madera, shatter cones also occur as fragments within polymict breccias, indicating these features form early, during the contact/compression stage of impact crater development. This observation was also noted from the Haughton structure, which contains shatter cone fragments within polymict breccia (Osinski and Spray, 2006). Magnetic studies of shatter cones from Sierra Madera indicate that magnetization in the carbonate rocks occurred in two phases corresponding to the initial compressive shock wave and an immediate decompression wave (Adachi and Kletetschka, 2008). These authors suggest that shatter cones at Sierra Madera formed during the second magnetization event, with localized melting along shatter cone surfaces (Adachi and Kletetschka, 2008). This event must have occurred early, during the contact/compression stage of crater development, for shatter cone clasts to be incorporated as clasts within polymict breccia.

What do the Deformational Features Reveal about Temperature and Pressure Conditions during the Impact Event?

It is difficult to use carbonate material as the sole means for determining pressure and temperature conditions during an impact event since rapidly quenched carbonate does not yield a uniquely deformed texture. However, using the shock classification scheme for impact metamorphosed sandstones developed by Kieffer (1971) and modified by Osinski (2007), we can assign shock pressure values to $CaCO_3$-cemented sandstones at Sierra Madera and apply those values to the adjacent carbonate units. Sandstones at Sierra Madera exhibit characteristics similar to Osinski's (2007) classes 2 and 3a for impact metamorphosed sandstone, which therefore provide a shock pressure range from ~3 to ~20 GPa

based on the presence of well-developed shatter cones, a "jigsaw" interlocking texture between quartz grains, and multiple sets of planar deformation features (PDFs) within quartz grains. This shock pressure range corresponds to a post-shock temperature range of 350 to >1000 °C (Kieffer, 1971; Osinski, 2007). Additionally, zircon deformational evidence indicates peak shock pressures were possibly ~20 GPa.

Sandstone units at Sierra Madera have a range of deformational features that do not increase toward the center of the central uplift or toward the region of expected highest shock. For example, the Cathedral Mountain Formation contains fewer deformational features than the sandstone from the Gilliam Limestone, even though it is more centrally located in the central uplift. This may indicate that shock pressure and temperature conditions were not distributed evenly during the impact event. The range of deformational features observed within the central uplift may also have been caused by movement of less shocked rocks upward during the formation of the central uplift and exposure by subsequent erosion. However, a recent XRD study of carbonate rocks at Sierra Madera documents an increase of peak broadening and dampening of peaks from samples on the crater rim to crater center (Huson et al., 2009). Broadening of XRD peaks and loss of peak intensity increases with increasing shock pressure (Skála and Jakeš, 1999). Samples from Sierra Madera indicate that carbonate rocks from the center of the central up-

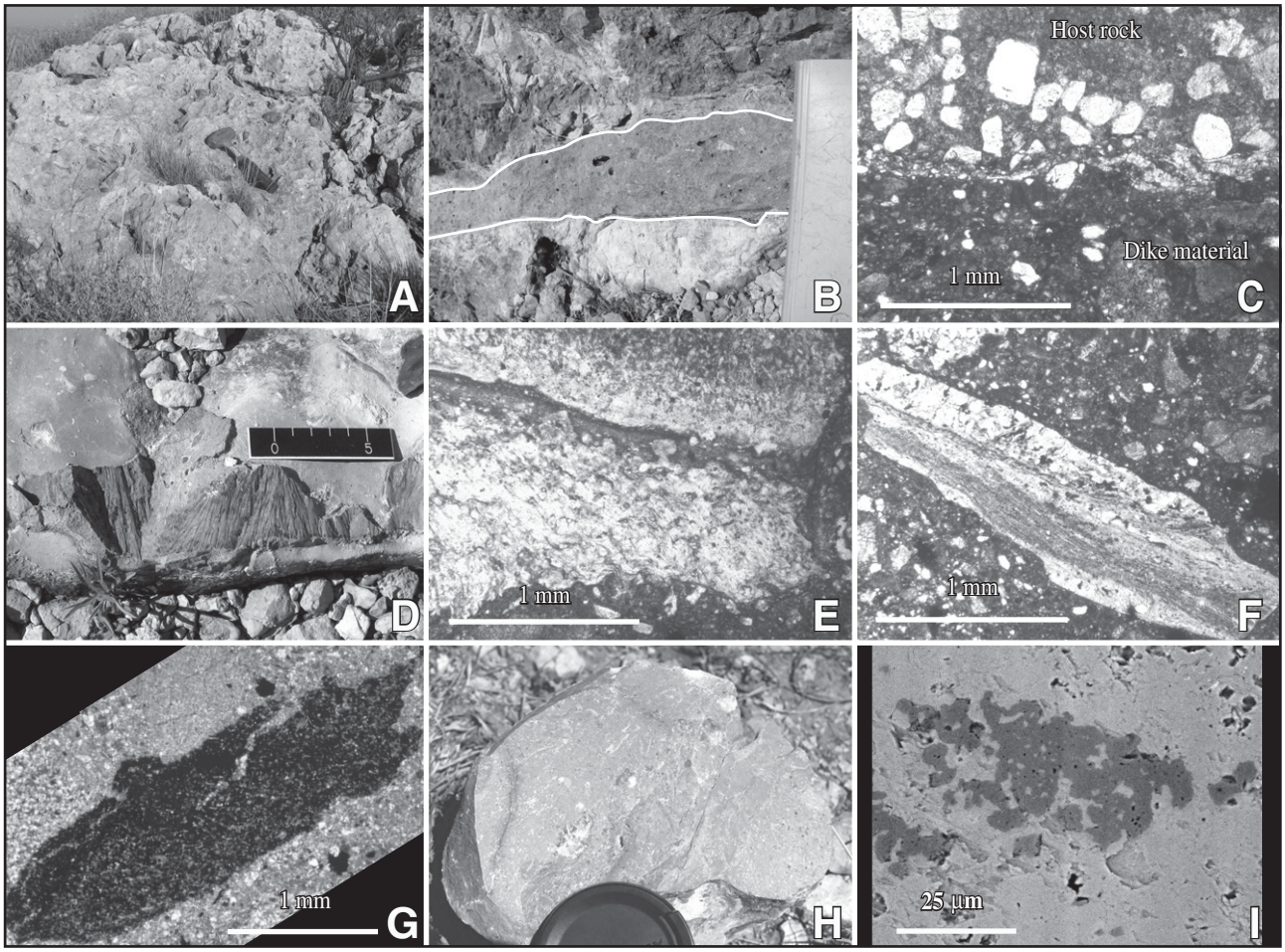

Figure 8. Polymict breccia outcrop and hand sample photographs. (A) Typical polymict breccia outcrop. Note hammer for scale. (B) Injection dike of polymict breccia into the Hess Formation outlined in white. Field book (right side of photo) is 15 cm in length. (C) Photomicrograph of an injection–dike-host-rock boundary. Plane-polarized light. (D) Polymict breccia with shatter cones in chert. Scale bar is 5 cm. (E) Photomicrograph of a partially melted sandstone clast within a polymict breccia. Note contorted layering and chaotic nature of the lower section of the clast compared to the undeformed upper section. Plane-polarized light. (F) Photomicrograph of a partially melted sandstone clast within a polymict breccia. Note flow within the lower melted section of the clast. Plane-polarized light. (G) Photomicrograph of a dark brown, altered glass clast within a polymict breccia sample. Plane-polarized light. (H) Photograph of fine-grained carbonate quench material. Lens cap is 5 cm in diameter. (I) Scanning electron microscope (SEM) image of rock in H. Possible immiscibility feature can be seen between carbonate material (light gray) and siliciclastic material (darker gray). Sample locations for these images are noted by square symbols on Figure 6: 15—Fig. 8A; 16—Fig. 8B; 17—Fig. 8C; 18—Fig. 8D; 19—Fig. 8E; 20—Fig. 8F; 21—Fig. 8G; 22—Fig. 8H, I.

lift are more highly shocked than those from the outer part of the central uplift. The discrepancy between shock characteristics in the sandstones and those of the carbonates within the central uplift may result from varying lithologic characteristics (i.e., porosity, matrix versus grain abundance, cement type, etc.) within the siliciclastic rocks, which might control the development of shock features within those rocks.

Amount of Deformation Observed in the Final Crater and Erosional Level within the Crater

The presence of centimeter-size injection dikes at Sierra Madera may indicate that this structure is deeply eroded below the crater floor, since breccia dikes are common in deeply eroded craters (Lambert, 1981). An additional indicator of a deeply eroded structure is the absence of an impact melt sheet, or in this case a suevite layer (for sedimentary structures; Kieffer and Simonds, 1980), within the ring depression. At Sierra Madera, evidence of an impact melt sheet or suevite was not observed during this study or previous studies (Wilshire et al., 1972). The melt sheet was eroded or is buried under sediment within the ring depression in the crater. However, the eroded crater rim, the presence of injection dikes, polymict and monomict breccia within the central uplift, and lack of abundant high-temperature deformational features indicate that the current surface at Sierra Madera is below the level at which the impact melt sheet would occur (Fig. 9; French, 1998). Additionally, past research suggests that erosion may have removed an estimated ~600 m (Wilshire et al., 1972) or ~700–1200 m (Goldin et al., 2006) of overlying material at Sierra Madera. Therefore, pressure and temperature estimates reported here (~3 to ~20 GPa pressure range and postshock temperature range of 350 to >1000 °C) should be considered low estimates of deformational conditions. Melt clasts within polymict breccia and carbonate melt locations observed in this study may have been injected downward through dikes and represent remnants of the higher temperature and pressure deformational regime that was eroded away.

An alternate hypothesis to the deep erosion ascribed here to the Sierra Madera structure is that it may have formed underwater (Kelly, 1966). A water-impact event would deform rocks immediately below the point of impact while leaving the crater rim moderately low or absent due to reworking of sediments by water surging back into the crater, as characterized by the Montagnais, Mjølnir, and Chesapeake Bay structures (Dypvik and Jansa, 2003). Additional evidence of a water impact includes resurge gullies eroded into the crater rim along with a thickening of fall-out breccia within the crater as the inflow of water collects and concentrates recently ejected materials. Postimpact crater modification by waves or currents will also lead to a flattening of central uplift peaks (Dypvik and Jansa, 2003).

CONCLUSIONS

Deformational features within the host rocks and impact-generated breccias were used to determine pressure and temperature conditions during the Sierra Madera impact event. Sandstones within the central uplift have a range of shock features. Shatter cones in sedimentary rocks indicate relatively low pressures, ~3 to ~20 GPa (Osinski, 2007). Planar features in zircon form from ~20 to ~60 GPa, whereas granular textures develop when shock pressures reach ~50 to ~70 GPa (Leroux et al., 1999; Wittmann et al., 2006). Planar microstructures within quartz form from ~5 to ~33 GPa (Osinski, 2007). Pressure conditions during the impact were at least 3 GPa from the presence of shatter cones but are possibly ~20 GPa based on planar fractures within shock-deformed zircon. Observations on the TEM scale would confirm the extent of shock damage zircon endured during the impact event. These pressures correspond to a postshock temperature range of 350 to >1000 °C (Osinski, 2007). The potential for higher deformational conditions remains due to removal of these features by erosion.

Varying lithologic characteristics of the rocks will influence the formation of shock features, possibly leading to the uneven distribution of shock characteristics observed within the sandstone units. Similarly, the distribution of shock features in sandstone may result from the uplift of deeper, less shocked stratigraphy. However, a study of shock-deformed carbonate indicates an increase in shock deformation toward the central uplift, supporting the shock response of sandstone to variable lithologic characteristics. It is therefore important to study both carbonate and siliciclastic shock deformation when determining the deformational history of well-eroded sedimentary impact structures.

ACKNOWLEDGMENTS

We would like to thank the Lyda and Lang Families for granting access to their property for sample collection. Also, the scanning electron microscope (SEM) used for the zircon work was made available by the Pacific Northwest National Laboratory in Richland, Washington. This research was supported by National Aeronautics and Space Administration (NASA) grant NNX06AE69G. Additional funding was provided by the Barringer Crater Company. This manuscript benefited from constructive reviews by Axel Wittmann, Ludovic Ferrière, and Christian Koeberl.

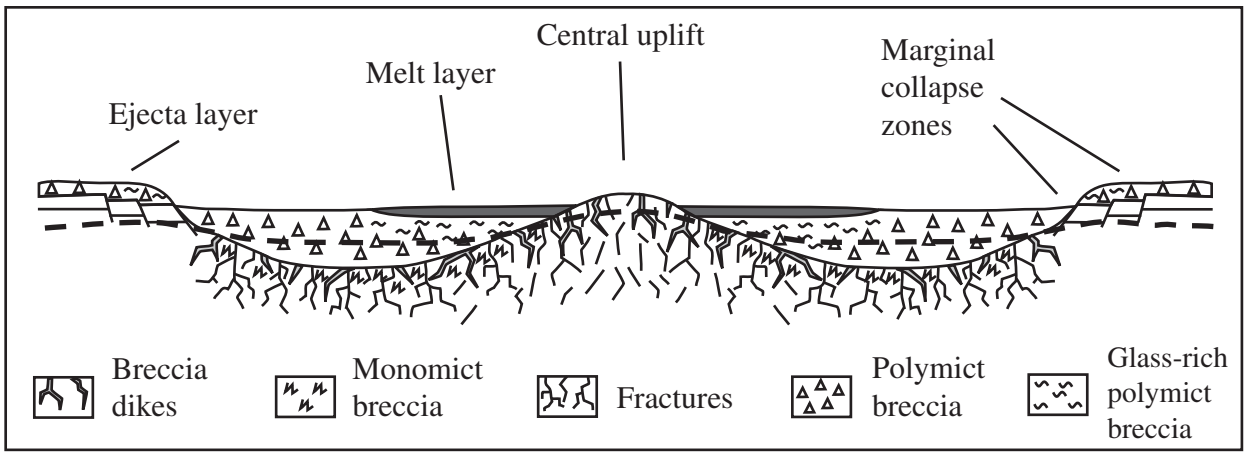

Figure 9. Complex impact crater showing impactite locations (modified from French, 1998). Dashed line in final complex crater indicates current erosional surface at Sierra Madera.

REFERENCES CITED

Adachi, T., and Kletetschka, G., 2008, Impact-pressure controlled orientations of shatter cone magnetizations in Sierra Madera, Texas, USA: Studia Geophysica et Geodaetica, v. 52, p. 237–254, doi: 10.1007/s11200-008-0016-0.

Austrheim, H., and Corfu, F., 2009, Formation of planar deformation features (PDFs) in zircon during coseismic faulting and an evaluation of potential effects on U-Pb systematics: Chemical Geology, v. 261, p. 25–31, doi: 10.1016/j.chemgeo.2008.09.012.

Bohor, B.F., Betterton, W.J., and Krogh, T.E., 1993, Impact-shocked zircons: Discovery of shock-induced textures reflecting increasing degrees of shock metamorphism: Earth and Planetary Science Letters, v. 119, p. 419–424, doi: 10.1016/0012-821X(93)90149-4.

Burt, J.B., Pope, M.C., and Watkinson, A.J., 2005, Petrographic, X-ray diffraction and electron spin resonance analysis of deformed calcite in the Kaibab Limestone, Meteor crater, Arizona: Meteoritics & Planetary Science, v. 40, p. 297–306, doi: 10.1111/j.1945-5100.2005.tb00381.x.

Dietz, R.S., 1960, Meteorite impact suggested by shatter cones in rock: Science, v. 131, p. 1781–1784, doi: 10.1126/science.131.3416.1781.

Dietz, R.S., 1968, Shatter cone in cryptoexplosion structures, *in* French, B.M., and Short, N.M., eds., Shock Metamorphism of Natural Materials: Baltimore, Maryland, Mono Book Corporation, p. 267–285.

Donelick, R.A., O'Sullivan, P.B., and Ketcham, R.A., 2005, Apatite fission track analysis, *in* Reiners, P.W., and Ehlers, T.A., eds., Low Temperature Thermochronology: Techniques, Interpretations, and Applications: Reviews in Mineralogy and Geochemistry, v. 58, p. 49–94.

Dypvik, H., and Jansa, L.F., 2003, Sedimentary signatures and processes during marine bolide impacts: A review: Sedimentary Geology, v. 161, p. 309–337, doi: 10.1016/S0037-0738(03)00135-0.

Eggleton, R.E., and Shoemaker, E.M., 1961, Breccia at Sierra Madera, *in* Short Papers in the Geologic and Hydrologic Sciences: U.S. Geological Survey Professional Paper 424-D, p. D151–D153.

Ferrière, L., Koeberl, C., Reimold, W.U., Hecht, L., and Bartosova, K., 2009, The origin of "toasted" quartz in impactites revisited [abs.], *in* 40th Lunar and Planetary Science Conference: Houston, Texas, Lunar and Planetary Institute abstract 1751.

French, B.M., 1998, Traces of Catastrophe: A Handbook of Shock-Metamorphic Effects in Terrestrial Meteorite Impact Structures: Lunar and Planetary Institute Contribution 954, 120 p.

Glass, B.P., and Liu, S., 2001, Discovery of high-pressure $ZrSiO_4$ polymorph in naturally occurring shock-metamorphosed zircons: Geology, v. 29, p. 371–373, doi: 10.1130/0091-7613(2001)029<0371:DOHPZP>2.0.CO;2.

Goldin, T.J., Wünnemann, K., Melosh, H.J., and Collins, G.S., 2006, Hydrocode modeling of the Sierra Madera impact structure: Meteoritics & Planetary Science, v. 41, p. 1947–1958, doi: 10.1111/j.1945-5100.2006.tb00462.x.

Graup, G., 1999, Carbonate-silicate liquid immiscibility upon impact melting: Ries crater, Germany: Meteoritics & Planetary Science, v. 34, p. 425–438, doi: 10.1111/j.1945-5100.1999.tb01351.x.

Grieve, R.A.F., and Pesonen, L.J., 1996, Terrestrial impact craters: Their spatial and temporal distribution and impacting bodies: Earth, Moon, and Planets, v. 72, p. 357–376, doi: 10.1007/BF00117541.

Grieve, R.A.F., and Robertson, P.B., 1979, The terrestrial cratering record: 1. Current status of observations: Icarus, v. 38, p. 212–229, doi: 10.1016/0019-1035(79)90179-9.

Grieve, R.A.F., Langenhorst, F., and Stöffler, D., 1996, Shock metamorphism of quartz in nature and experiment: II. Significance in geoscience: Meteoritics & Planetary Science, v. 31, p. 6–35.

Haneef, M., and Wardlaw, B.R., 2000, Lithofacies and depositional history of the Tessey Formation, Frenchman Hills, west Texas, *in* Wardlaw, B.R., Grant, R.E., and Rohr, D.M., eds., The Guadalupian Symposium: Smithsonian Contributions to the Earth Sciences, v. 32, p. 373–380.

Hill, C.A., 1996, Geology of the Delaware Basin Guadalupe, Apache, and Glass Mountains New Mexico and West Texas: Society of Economic Paleontologists and Mineralogists, Permian Basin Section, Publication 96–39, 480 p.

Howard, K.A., and Offield, T.W., 1968, Shatter cones at Sierra Madera, Texas: Science, v. 162, no. 3850, p. 261–265, doi: 10.1126/science.162.3850.261.

Howard, K.A., Offield, T.W., and Wilshire, H.G., 1972, Structure of Sierra Madera, Texas, as a guide to central peaks of lunar craters: Geological Society of America Bulletin, v. 83, p. 2795–2808, doi: 10.1130/0016-7606(1972)83[2795:SOSMTA]2.0.CO;2.

Huson, S.A., Pope, M.C., Watkinson, A.J., and Foit, F.F., 2005, Possible planar elements in zircon as indicator of peak impact pressures from the Sierra Madera impact crater, West Texas [abs.], *in* Lunar and Planetary Science Conference XXXVI: Lunar Planetary Institute, Houston, Texas, abstract 2048.

Huson, S.A., Foit, F.F., Watkinson, A.J., and Pope, M.C., 2009, Rietveld analysis of X-ray powder diffraction patterns as a potential tool for the identification of impact deformed rocks: Meteoritics & Planetary Science, v. 44, p. 1695–1706, doi: 10.1111/j.1945-5100.2009.tb01200.x.

Kalleson, E., Corfu, F., and Dypvik, H., 2009, U-Pb systematics of zircon and titanite from the Gardnos impact structure, Norway: Evidence for impact at 546 Ma?: Geochimica et Cosmochimica Acta, v. 73, p. 3077–3092, doi: 10.1016/j.gca.2009.02.020.

Kelly, A.O., 1966, A water-impact hypothesis for the Sierra Madera structure in Texas: Meteoritics, v. 3, no. 2, p. 79–82.

Kieffer, S.W., 1971, Shock metamorphism of the Coconino sandstone at Meteor crater, Arizona: Journal of Geophysical Research, v. 76, p. 5449–5473, doi: 10.1029/JB076i023p05449.

Kieffer, S.W., and Simonds, C.H., 1980, The role of volatiles and lithology in the impact cratering process: Reviews of geophysics and space physics, v. 18, no. 1, p. 143–181.

Kieffer, S.W., Phakey, P.P., and Christie, J.M., 1976, Shock processes in porous quartzite: Transmission electron microscope observations and theory: Contributions to Mineralogy and Petrology, v. 59, p. 41–93, doi: 10.1007/BF00375110.

Lambert, P., 1981, Breccia dikes: Geological constraints on the formation of complex craters, *in* Schultz, P.H., and Merrill, R.B., Multi-Ring Basins: Proceedings of the Lunar and Planetary Science Conference, v. 12A, p. 56–78.

Leroux, H., Reimold, W.U., Koeberl, C., Hornemann, U., and Doukhan, J.C., 1999, Experimental shock deformation in zircon: A transmission electron microscope study: Earth and Planetary Science Letters, v. 169, p. 291–301, doi: 10.1016/S0012-821X(99)00082-5.

Mänttäri, I., and Koivisto, M., 2001, Ion microprobe uranium-lead dating of zircons from the Lappajärvi impact crater, western Finland: Meteoritics & Planetary Science, v. 36, p. 1087–1095, doi: 10.1111/j.1945-5100.2001.tb01946.x.

Metzler, A., Ostertag, R., Redeker, H.J., and Stöffler, D., 1988, Composition of the crystalline basement and shock metamorphism of crystalline and sedimentary target rocks at the Haughton impact crater: Meteoritics, v. 23, p. 197–207.

Nicolaysen, L.O., and Reimold, W.U., 1999, Vredefort shatter cones revisited: Journal of Geophysical Research, v. 104, no. B3, p. 4911–4930, doi: 10.1029/1998JB900068.

Osinski, G.R., 2007, Impact metamorphism of $CaCO_3$-bearing sandstones at the Haughton structure, Canada: Meteoritics & Planetary Science, v. 42, p. 1945–1960, doi: 10.1111/j.1945-5100.2007.tb00552.x.

Osinski, G.R., and Spray, J.R., 2001, Impact generated carbonate melts: Evidence from the Haughton structure, Canada: Earth and Planetary Science Letters, v. 194, p. 17–29, doi: 10.1016/S0012-821X(01)00558-1.

Osinski, G.R., and Spray, J.R., 2006, Shatter cones of the Haughton impact structure, Canada, *in* Proceedings of the 1st International Conference on Impact Cratering in the Solar System: European Space Agency Special Publication SP-612 (CD-ROM).

Rohr, D.M., Miller, J.M., Davis, R.A., and Mamay, S.H., 1982, An Upper Permian (Guadalupian) flora from the Glass Mountains area, Brewster County, west Texas (abs): Geological Society of America Abstracts with Programs, v. 14, p. 602.

Ross, C.A., 1986, Paleozoic evolution of southern margin of Permian Basin: Geological Society of America Bulletin, v. 97, p. 536–554, doi: 10.1130/0016-7606(1986)97<536:PEOSMO>2.0.CO;2.

Short, N.M., and Gold, D.P., 1996, Petrography of shocked rocks from the central uplift at the Manson impact structure, *in* Koeberl, C., and Anderson R.R., eds., The Manson Impact Structure, Iowa: Anatomy of an Impact Crater: Geological Society of America Special Paper 302, p. 245–265.

Skála, R., and Jakeš, P., 1999, Shock-induced effects in natural calcite-rich targets revealed by X-ray powder diffraction, *in* Dressler, B.O., and Sharpton, V.L., Large Meteorite Impacts and Planetary Evolution II: Geological Society of America Special Paper 339, p. 205–214.

Stöffler, D., and Grieve, R.A.F., 2007, Impactites, chapter 2.11, *in* Fettes, D., and Desmons, J., eds., Metamorphic Rocks: A Classification and Glossary of Terms; Recommendations of the International Union of Geological Sciences Subcommission on the Systematics of Metamorphic Rocks: Cambridge, UK, Cambridge University Press, p. 82–92, 111–125, and 126–242.

Stöffler, D., and Langenhorst, F., 1994, Shock metamorphism in nature and experiment: I. Basic observation and theory: Meteoritics, v. 29, p. 155–181.

Stöffler, D., Bischoff, L., Oskierski, W., and Wiest, B., 1988, Structural deformation, breccia formation, and shock metamorphism in the basement of complex terrestrial impact craters: Implications for the cratering products, *in* Bodén, A., and Eriksson, K.G., eds., Deep Drilling in Crystalline Bedrock: Volume 1. The Deep Gas Drilling in the Siljan Impact Structure, Sweden, and Astroblemes: New York, Springer-Verlag, p. 277–297.

Tuchscherer, M.G., Reimold, W.U., Koeberl, C., Gibson, R.L., and de Bruin, D., 2004, First petrographic results on impactites from the Yaxcopoil-1 borehole, Chicxulub structure, Mexico: Meteoritics & Planetary Science, v. 39, no. 6, p. 899–930, doi: 10.1111/j.1945-5100.2004.tb00937.x.

Wardlaw, B.R., Davis, R.A., Rohr, D.M., and Grant, R.E., 1990, Leonardian-Wordian (Permian) deposition in the northern Del Norte Mountains, west Texas: U.S. Geological Survey Bulletin 1881, p. A1–A14.

Warme, J.E., 2004, The many faces of the Alamo impact breccia: Geotimes, v. 49, no. 1, p. 26–29.

Warme, J.E., and Kuehner, H.C., 1998, Anatomy of an anomaly; the Devonian catastrophic Alamo impact breccia of southern Nevada, *in* Ernst, W.G., and Nelson, C.A., eds., Integrated Earth and Environmental Evolution of the Southwestern United States; the Clarence A. Hall, Jr. Volume: Columbia, Maryland, Bellweather Publishing, p. 80–107.

Whitehead, J., Spray, J.G., and Grieve, R.A.F., 2002, Origin of "toasted" quartz in terrestrial impact structures: Geology, v. 30, no. 5, p. 431–434, doi: 10.1130/0091-7613(2002)030<0431:OOTQIT>2.0.CO;2.

Wieland, F., Reimold, W.U., and Gibson, R.L., 2006, New observations on shatter cones in the Vredefort impact structure, South Africa, and evaluation of current hypotheses for shatter cone formation: Meteoritics and Planetary Science, v. 41, no. 11, p. 1737–1759.

Wilshire, H.G., and Howard, K.A., 1968, Structural pattern in central uplifts of cryptoexplosion structures as typified by Sierra Madera: Science, v. 162, no. 3850, p. 258–261, doi: 10.1126/science.162.3850.258.

Wilshire, H.G., Offield, T.W., Howard, K.A., and Cummings, D., 1972, Geology of the Sierra Madera cryptoexplosion structure, Pecos County, Texas: U.S. Geological Survey Professional Paper 599-H, p. 1–49.

Wittmann, A., Kenkmann, T., Schmitt, R.T., and Stöffler, D., 2006, Shock-metamorphosed zircon in terrestrial impact craters: Meteoritics & Planetary Science, v. 41, no. 3, p. 433–454, doi: 10.1111/j.1945-5100.2006.tb00472.x.

Manuscript Received 23 September 2009
Revised Manuscript Received 27 January 2010
Manuscript Accepted 29 January 2010

Printed in the USA